Asymmetric polybenzimidazole membranes with thin selective skin layer containing ZIF-8 for H_2/CO_2 separation at pre-combustion capture conditions

Javier Sánchez-Laínez, Beatriz Zornoza, Carlos Téllez and Joaquín Coronas**

Chemical and Environmental Engineering Department, Instituto de Nanociencia de Aragón (INA), Universidad de Zaragoza, 50018 Zaragoza, Spain. Email: bzornoza@unizar.es, coronas@unizar.es

Abstract: This work addresses an optimization in the fabrication of flat PBI membranes containing ZIF-8 nanoparticles for gas separation purposes. The PBI membranes were prepared in an asymmetric configuration on P84® supports, representing a new way of preparing flat PBI membranes. An optimization of the conditions for the PBI phase inversion preparation method, including the dope composition (in the 15-26 wt% range), has been carried out to obtain PBI membranes with a 1 μm selective skin layer. The asymmetric membranes showed an unprecedented gas separation capacity in pre-combustion CO_2 capture, much superior to dense membranes, under harsh operating conditions (250 °C and 6 bar feed), performing up to 20.3 GPU of H_2 and a H_2/CO_2 selectivity of 35.6. Their much thinner selective layer made possible the increase in selectivity because of the saturation of the CO_2 flow at high pressures. The reduction in the amount of ZIF-8 for obtaining a membrane with the same filler loading (3.7 vs. 9.3 g/m^2) was also possible. The activation energy of the membranes, as well as the flow resistances, were calculated, providing a resistance in series model to understand the flow inside the membrane.

***Keywords*:** CO_2 capture; asymmetric membrane; polybenzimidazole; metal-organic-framework.

1. Introduction

Carbon capture and storage *via* pre-combustion processes involve the separation of H_2/CO_2 mixtures with a high CO_2 concentration (~45 vol %) at elevated pressure (15−20 bar) and temperature (190−210 °C) [1]. This mixture is the result of syngas generation from the steam reforming of hydrocarbon sources such as natural gas, heavy oils and naphtha, coal or biomass. The whole process consists of three steps: the catalytic reforming of methane, a water gas shift reaction and the purification of the resulting hydrogen flow [2]. Purification is needed to capture the CO_2, leaving a stream of nearly-pure hydrogen that will be burned in a combined cycle power plant to generate electricity [3]. In view of the high CO_2 concentration, pre-combustion capture is more efficient than post-combustion, but the severe operating conditions make the separation process more complicated.

Various approaches can be employed for CO_2 separation such as pressure swing adsorption, temperature swing adsorption and cryogenic distillation. However, membrane technology appears to be a more efficient alternative thanks to its attractive properties: simplicity, ease of operation, and versatility for a large number of potential uses. Besides, hydrogen separation is suited to membrane technology as hydrogen has a very high permeation rate relative to most other gases due to its small kinetic diameter, and thus its high diffusivity.

Currently, polymeric membranes rule the commercial scene for CO_2 capture. Very recently, Pinnau's group developed thin skin membranes by interfacial polymerization, able to reach a H_2 permeance of 500 GPU and a H_2/CO_2 selectivity of 50 [4]. However, these membranes could only withstand temperatures up to 140 ^{0}C due to the use of polysulfone supports. Pre-combustion capture needs membranes produced from materials with a high mechanical and thermal stability due to the harsh operating conditions involved. Polybenzimidazole (PBI) is a polymer with inherent mechanical, physical and chemical stability. This material retains its robustness up to 600-630 ^{0}C [5] and has a high glass transi-

tion temperature (427 ^{0}C) [6]. Furthermore, the high chain packing density of this material provides diffusivity selectivity at temperatures above 150 ^{0}C. However, its major drawbacks are low permeability and brittleness [7].

Polymeric membranes can be classified as symmetric or asymmetric according to their morphology [8]. Symmetric membranes constitute a dense or porous continuous matrix. They are prepared by evaporation of the casting solution and all their thickness is selective for gas separation. The main disadvantage of these membranes is their high resistance to flow, resulting in low flow rates and therefore low feasibility for commercial applications. Asymmetric membranes have a heterogeneous morphology. They consist of a dense layer integrally formed over a porous layer. The porous substructure provides mechanical support and prevents the membrane from breaking, whereas the dense skin layer is responsible for molecular discrimination and flow resistance. Such membranes are normally prepared in one step following the phase inversion technique developed by Loeb and Sourirajan [9], which consists of the precipitation of a casting solution by immersion in a non-solvent bath.

The use of PBI membranes for the separation of H_2/CO_2 mixtures has been widely reported in the form of flat dense membranes [10-20] and hollow fibers [21-25]. Although flat asymmetric PBI membranes can be found in the literature for applications such as nanofiltration or forward osmosis [26-28], they are not so developed for gas separation purposes. Only a few reports of gas separation with flat asymmetric membranes made from other polymers can be found in the literature [29-34].

This study provides a method for the preparation of defect-free flat asymmetric PBI membranes, showing their yet to be developed potential for the separation of H_2/CO_2 mixtures at high temperature and pressure. The membranes were prepared over non-selective polyimide P84® to provide mechanical strength to the composite. The results were compared with those of dense PBI films reported in previous studies and self-supported membranes. Moreover, ZIF-8 has also been embedded in the PBI phase with

the aim of enhancing the gas separation properties of the membranes. ZIF-8 is a zeolitic imidazolate framework (a kind of metal-organic framework), with Zn cations coordinated to 2-methylimidazolate (2-mIm) ligands. It has the **sod** zeolitic topology with cavities of 1.16 nm connected through smaller windows of 0.34 nm. This ZIF has been widely reported in the literature for the preparation of mixed matrix membranes (MMMs) for gas separation [15,19,35,36].

2. Experimental Section

2.1 Materials

Zinc nitrate hexahydrate ($Zn(NO_3)_2 \cdot 6H_2O$), 2-methylimidazole (mIm, $C_4H_6N_2$, >99%) and N,N-Dimethylacetamide (DMAc) were purchased from Sigma Aldrich. Methanol (MeOH, HPLC grade), isopropyl alcohol (IPA, 99.5%) and n-hexane were purchased from Scharlau. Commercial PBI solution comprising 26 wt% PBI with 1.5 wt% LiCl as stabilizer in DMAc solvent was purchased from PBI Performance Products and P84® was purchased from HP polymer GmbH.

2.2 ZIF-8 nanoparticle synthesis

This ZIF synthesis was adapted from the literature [37]. 0.47 g of zinc nitrate hexahydrate ($Zn(NO_3)_2 \cdot 6H_2O$, >98%, Sigma Aldrich) was dissolved in 10 mL of MeOH (Scharlau) and 10 mL of deionized (DI) water. Besides, 1.0 g of mIm was dissolved in 10 mL of MeOH, and the two solutions were mixed and stirred for 2 h. The final product was collected by centrifugation, washed once with MeOH, and dried at 110 ^{0}C overnight. The resulting nanoparticles had an average size of 150 nm.

2.3 Preparation of P84® asymmetric supports

Asymmetric porous P84® supports were prepared following the phase inversion method. A 23 wt% dope solution of P84® was prepared, dissolving the corresponding amount of powder in DMAc. The polymer solution was cast onto a glass plate using an Elcometer 4340 Automatic Film Applicator placed in a fume hood and immediately immersed into a tap water bath at 25 ^{0}C. After precipitation, the membranes were kept in a DI water bath overnight and then rinsed with IPA in order to remove the remaining DMAc. The films were dried at 100 ^{0}C for one day prior to use [38].

2.4 PBI asymmetric membrane preparation

PBI asymmetric membranes were also prepared following the phase inversion method. A 20 wt% dope solution was directly obtained by diluting the 26 wt% PBI commercial solution in DMAc. The casting solution was left still overnight to remove any bubbles. The polymer solution was cast onto a P84® support using the same device as for the P84® films and immediately immersed into a DI water bath at 25 ^{0}C. After precipitation, the membranes were kept in a DI water bath for three days in order to remove all the DMAc. The membranes were then rinsed in MeOH and n-hexane for 90 min each, before drying at room temperature. Once dried, the membranes were healed following a dip coating method. The coating solution was prepared mixing PDMS polymer base and hardener with a weight ratio of 10 to 1. The mixture was added to n-hexane to obtain a 3 wt% solution. The membranes were immersed in the coating solution for 5 min, and then allowed to evaporate at room temperature for 2h. Finally, the membranes were cured in an oven at 100 ^{0}C for 18 h, resulting in a coated PDMS film of around 500 nm thickness. PBI membranes containing ZIF-8 were prepared analogously. In this case, ZIF-8 nanoparticles were dispersed in DMAc and commercial PBI solution (26 wt%) was added in three steps until a 20 wt% dope solution was obtained. As reported by Wang et al. [39], the PBI dope was selected near the critical concentration, obtained plotting the viscosity-concentration values from PBI Performance Prod-

ucts data (Fig. S1) [40]. A concentration near this critical value is necessary so that a thin skin layer with fewer defects can be formed [41]. Moreover, dopes with a PBI concentration of 15 and 26 wt% were also used to prepare membranes for characterization. These PBI self-supported membranes were also prepared on a glass plate, following the same procedure as for the P84® supports.

2.5 Membrane characterization

Thermogravimetric analyses (TGA) were carried out using a Mettler Toledo TGA/STDA 851e. Samples (10 mg) placed in 70 µL alumina pans were heated in an air flow of 40 mL from 25 to 900 ^{0}C at a heating rate of 10 ^{0}C/min. Scanning electron microscopy (SEM) images of MOFs and membranes were obtained using a FEI Inspect F50 model SEM, operated at 20 kV. Cross-sections of membranes were prepared by freeze-fracturing after immersion in liquid N_2 and subsequently coated with Pt. Membranes were also characterized by Raman spectroscopy using a WiTec Alpha300 Confocal Raman Microscope, with a 785 nm laser excitation beam. Carbon dioxide adsorption isotherms were measured using a volumetric adsorption analyzer (Micromeritics ASAP 2020) at 273K up to 120 kPa after degassing at 200 ^{0}C for 8 h. In all cases, the hydrogen, carbon dioxide and helium gases used in the experiments were 99.9995% pure.

2.6 Gas separation performance

The membrane samples were placed in a module consisting of two stainless steel pieces and a 316LSS macroporous disk support of 3.14 cm^2 (from Mott Co.) with a 20 µm nominal pore size, and gripped inside with silicon O-rings. The permeation module was placed in a UNE 200 Memmert oven to control the temperature of the experiments. Gas separation measurements were carried out by feeding a H_2/CO_2 equimolar mixture (25/25 cm^3(STP)/min) from 3 to 6 bar to the feed side by means of two mass-flow controllers (Alicat Scientific, MC-100CCM-D), while the permeate side of the membrane

was swept with a 2-10 cm^3(STP)/min mass-flow controlled stream of Ar at 1 bar. Concentrations of H_2 and CO_2 in the outgoing streams were analyzed by an Agilent 3000A online gas microchromatograph equipped with a thermal conductivity detector. Permeation was calculated in GPU (10^{-6} cm^3(STP)/(cm^2·s·cmHg)) once the steady-state of the exit stream was reached (after at least 3 h), and the separation selectivity was calculated as the ratio of permeances. At least 2-3 membrane samples of each type were fabricated and measured to provide the corresponding error estimations.

3. Results and discussion

3.1 Membrane characterization

The SEM images in Fig. 1 reveal how the polymer concentration of the casting solution has an effect on the differentiation and thickness of the selective skin layer and porous sponge substructure. The distance from the top of the finger-like macropores to the external part of the membranes is approximately 0.5, 1 and 19 µm when using PBI dopes of 15, 20 and 26 wt%, respectively. As seen in Fig. 1d, this increase follows an exponential trend, like the polymer solution viscosity with increasing concentration (fitting from the data of Fig. S1). Both fitting equations can be seen in Fig. S2. The polymer concentration also had an effect on the substructure and thus on the mechanical strength of the membrane, because only self-supported membranes prepared from 26 wt% dope solutions could be measured for gas separation. The rest of membranes were too brittle to support the feed pressure. The absence of a bore fluid, as used for hollow fiber fabrication [42], made the fingers (i.e. the large columnar macropores) grow from the bottom of the membrane, turning it into a fragile structure. Besides, the quantity of finger-like macropores decreased at high PBI concentrations, resulting in a denser membrane with the consequent reduction in permeation. Due to the brittleness of PBI, it was necessary to support the membranes on a polymeric substrate able to resist the handling for further characterization and the high temperatures and pressures of the gas separation test. Polyimide P84® was chosen since it is a high

performance reliable polymer that has already been used as an inner layer in PBI hollow fibers [42]. Moreover, our research group has a wide knowledge of P84® flat supports for nanofiltration issues [43,44].

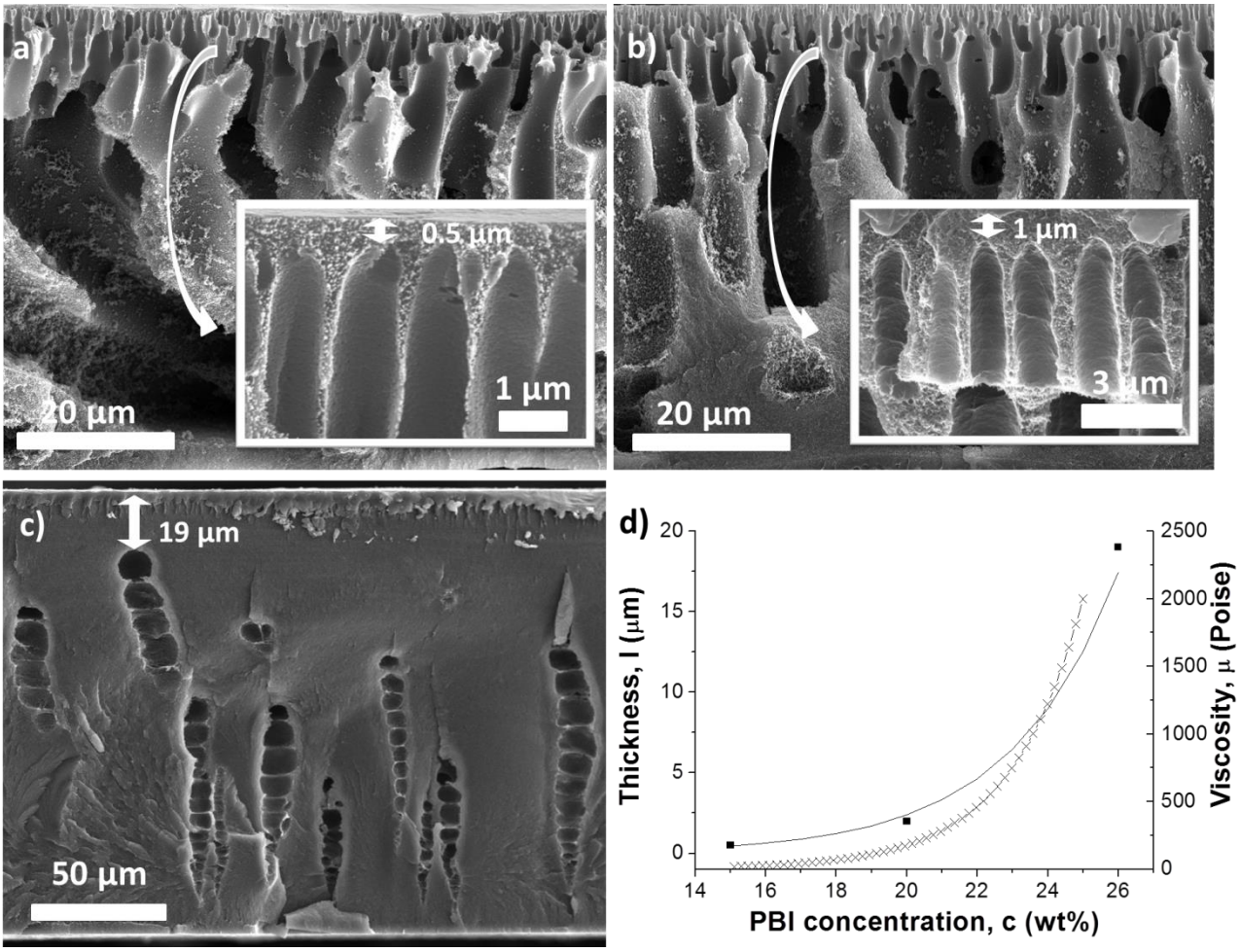

Figure. 1. SEM images of the cross-section of PBI self-supported asymmetric membranes fabricated from PBI dopes at 15 wt% (a), 20 wt% (b) and 26 wt% (c). PBI membrane skin layer thickness and PBI solution viscosity at 25 °C as function of PBI concentration in DMAc (d).

Fig. 2 (left) shows the Raman spectra of the cross-section of a PBI supported membrane. Different points on zones corresponding to the PBI, the PBI/P84® interface and the P84® support were measured. The PBI Raman spectrum shows weak signals owing to fluorescence at lower Raman shifts. The band at 549-694 cm^{-1} is attributed to C–H out-of-plane ring deformation. The signals at 1374 and 1617

cm^{-1} are attributed to C–H in-plane bending vibrations and C=C/C=N benzimidazole ring stretching vibrations, respectively [45]. The P84® spectrum shows intense peaks in the 1000-1600 cm^{-1} band. The signal at 1535 and 1592 cm^{-1} corresponds to aromatic C-C stretching. The band at 1012 cm^{-1} is related to the C-H in-plane bending mode and that at 1290 cm-^{1} to the C=O in-phase stretching mode [46]. Signals of PBI cannot be distinguished in the interphase spectrum due to their low intensity, and only those of P84® are visible. Fig. 2 (right) shows the SEM image of this cross-section. The P84® support has a thickness of around 120 µm while the PBI film only of 30 µm (20 wt% PBI dope). The P84® support is constituted by two different porous layers, finger-like macropores and a ca. 15 µm thick porous sponge above them. No delamination can be observed at the interface between the two layers, indicating a good adhesion. This makes sense since PBI and P84® are highly compatible at molecular level [47]. The upper zone of the PBI layer reveals a dense structure at a high magnification (Fig. 2 inset), corresponding to the selective skin layer, while the inner zone is very porous, which is desirable for minimizing the transport resistance.

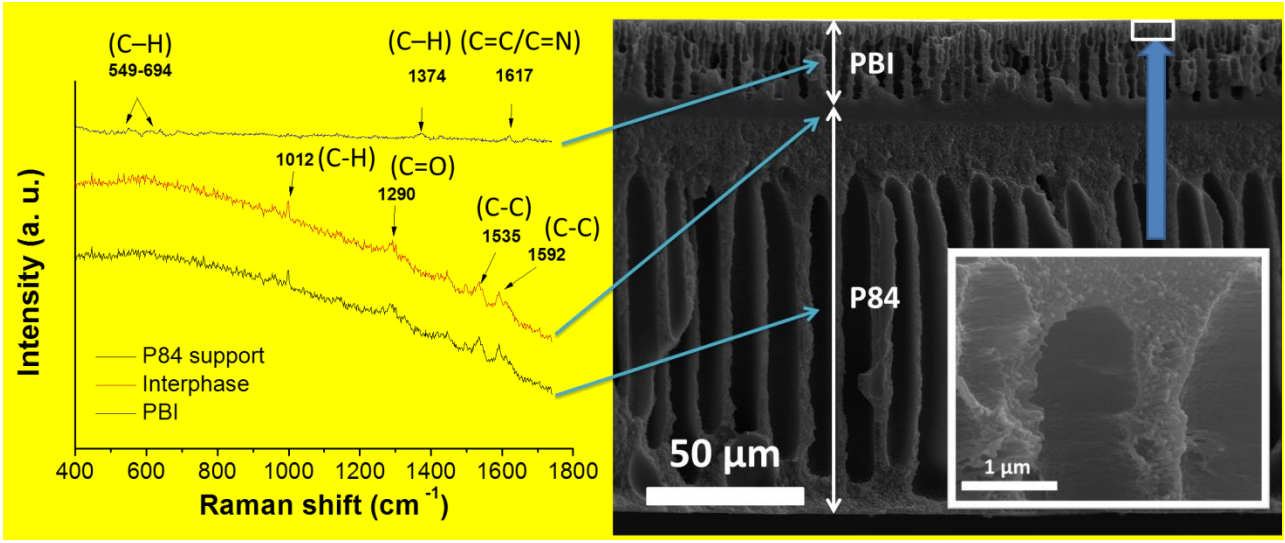

Figure. 2. Raman spectra on different zones of the cross-section of a PBI supported membrane (left) together with its SEM image (right) with a zoom into the PBI skin layer (inset). The membrane was prepared from a 20 wt% PBI dope.

The thermal stability of supported PBI membranes was tested by thermogravimetric analysis in air (see Fig. S3). The membrane was stable up to 400 ^{0}C, making it suitable for H_2 separation at high temperature. Despite containing two different polymers, PBI as selective layer and P84® as support, the TGA obtained was a continuous curve in which it is difficult to distinguish one from the other. The major proportion of P84® in the composite is responsible for this behavior.

In order to improve the gas separation performance of the PBI asymmetric films, ZIF-8 was embedded into the PBI polymeric phase to form 10 wt% loaded MMMs, calculated from the TGA results of Fig. S4. The SEM images of cross-sections of these membranes (Fig. 3) reveal the presence of ZIF-8 nanoparticles in the PBI section over the P84® support (see arrows in inset). ZIF-8 nanoparticles were verified by EDX analysis (see Fig. 3 inset). The thin selective layer of PBI asymmetric membranes allowed the reduction in the necessary amount of ZIF-8 to prepare this kind of MMMs to 3.7 g/m^2. This means a 2.5 fold decrease in comparison with the value for obtaining an 80 µm dense membrane with the same filler loading (9.3 g/m^2).

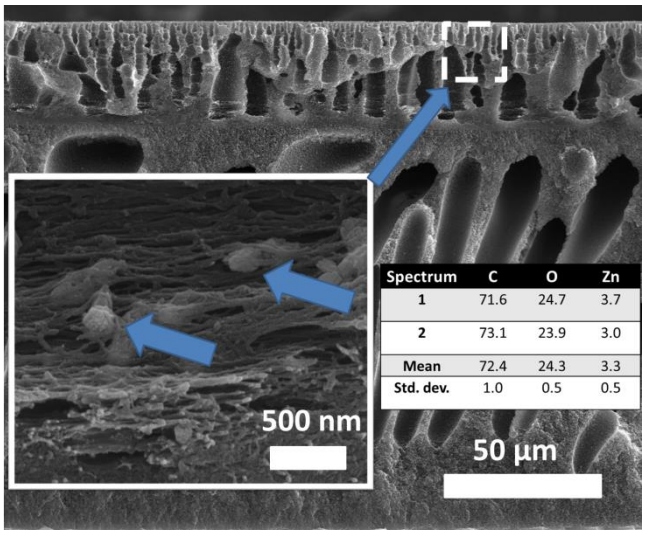

Figure. 3. SEM image of the cross-section of a supported PBI asymmetric MMM with 10 wt% loading of ZIF-8 including EDX analysis (inset).

3.2 Permeation results: dense vs. asymmetric PBI membranes

The P84® supports had no H_2/CO_2 selectivity when tested for gas separation. The use of a dope concentration below the critical value [25] prevents the formation of a selective skin layer and makes the films suitable for use as low resistant, non-selective supports for PBI membranes.

Fig. 4a shows the gas separation performance at 180 °C of dense PBI membranes (data from [20]) and four different PBI asymmetric membranes: self-supported membranes prepared from a 26 wt% concentration PBI dope (as seen above, lower concentration dopes gave rise to non-mechanically resistant membranes), supported membranes prepared from a 20 wt% dope before and after coating with PDMS, and ZIF-8 MMMs healed with PDMS. The mean and standard deviation values corresponding to the measurement of 2-3 different membranes can be seen in Table S1.

The preparation of membranes *via* phase inversion resulted in an improvement in the H_2/CO_2 selectivity (9.5) in comparison with dense membranes prepared by evaporation (3.0), reaching values up to four-fold higher. The differences in these two values indicate that the polymer structure is different in the skin layer of the asymmetric membrane compared to that of the dense membrane. This can be associated to polymer molecular orientation or the motion of polymer chains [48]. As a result, the micropore volume of the skinned dense polymer is lower than that of the intrinsic material. It is worth noting that supported PBI membranes still have defects that need healing with PDMS since their selectivity is lower (7.9) than that of self-supported membranes, although the coating with PDMS also implies a substantial reduction in the H_2 permeance (with a better selectivity of 12.6). These defects may be related to the proximity of macrovoids to the outer surface of the membranes [21]. In any event, repairing techniques are usually employed to achieve effective membranes for practical applications [49]. As expected, H_2 permeance is higher for the asymmetric membranes due to the lower thickness of their selective layers, with maximum values of 15.2 GPU against the 0.32 GPU of dense PBI (with ca. 80 μm thickness). Regarding the MMMs, embedding ZIF-8 into the PBI matrix has a positive effect on the membrane per-

formance. The H_2 permeance doubles in comparison with the value of the PBI membranes repaired with PDMS, and the H_2/CO_2 selectivity is 13 % higher, reaching a value of 14.5. These membranes also show a better performance than that of ZIF-8/PBI hollow fibers found in the literature [35].

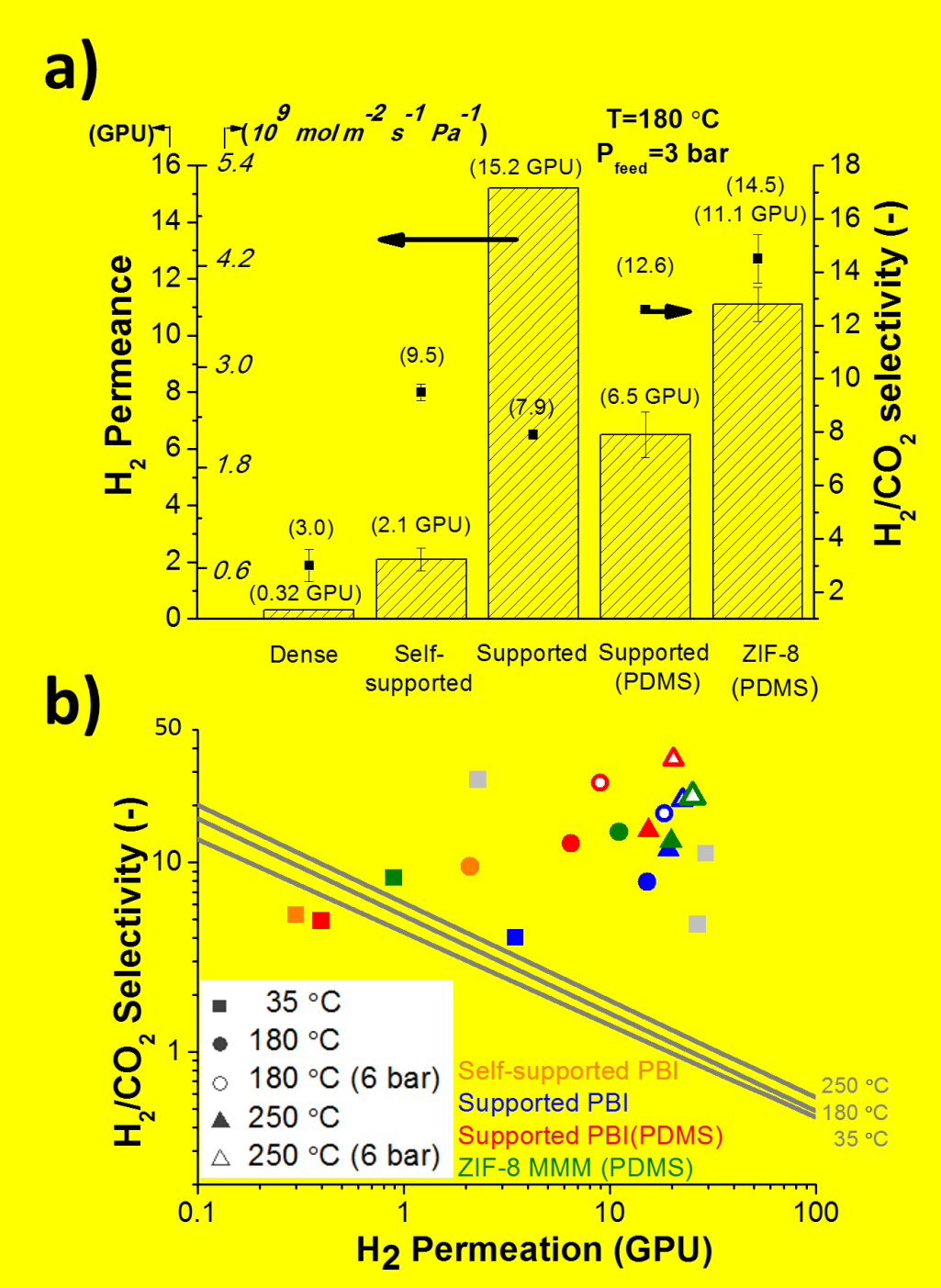

Figure. 4. Gas separation performance of dense PBI, self-supported asymmetric PBI, supported asymmetric PBI and asymmetric ZIF-8 10 wt% MMM. Histogram at 180 ^{0}C with feed and permeate pressures of 3 and 1 bar, respectively (a), and upper-bound plot (from 35 to 250 ^{0}C and pressure from 3 to 6 bar) with a comparison with hollow fiber literature values (in grey)[24-26] (b).

3.3 Influence of the temperature on the gas separation performance

The different PBI asymmetric membranes were tested at temperatures of 35, 180 and 250 ^{0}C. Their gas separation performances can be seen in the permeance-selectivity graph in Fig. 4b together with the literature values for PBI hollow fibers, given that no results for flat asymmetric membranes with this polymer have been published to date. Since the Robeson upper-bound [50] was originally defined for dense membranes at 35°C, single gas permeability was set in Barrer. However, this unit is useless for asymmetric membranes, where the thickness of the selective thin layer is unknown. We have calculated an H_2/CO_2 upper-bound relationship in GPU, using the values from the literature that defined the original upper-bound but changing the permeation values from Barrer to GPU (see Table S2 and Fig. S5). As the temperature has an influence on the upper-bound (Eq. S1), we have also calculated the corresponding upper-bounds at 180 and 250 ^{0}C (Eq. S2 and S3). At 35 °C, supported PBI membranes surpassed the H_2/CO_2 upper-bound, as did all the membranes at high temperatures. Moreover, PBI supported membranes have superior permeation and selectivity than self-supported membranes once healed with PDMS. For example, at 180 ^{0}C and 3 bar of feed pressure they showed 6.5 GPU of H_2 and a H_2/CO_2 selectivity of 12.6. This means that the H_2 permeation was three-fold higher and the selectivity 25% higher in comparison with self-supported PBI. When increasing the temperature to 250 ^{0}C at the same feed pressure, PBI supported membranes showed values of 14.4 GPU of H_2 and a H_2/CO_2 selectivity of 13.8 at 3 bar. Increasing the feed pressure also had a positive influence on the membranes gas separation performance, which will be discussed in the following section. It can be seen in Fig. 4b how

the literature values agree with our experimental results, despite referring to hollow fiber membranes. This is indicative of the huge gas permeance obtained using an asymmetric configuration.

In the case of ZIF-8/PBI asymmetric MMMs, Fig. 4b depicts how the H_2 permeance is at least one and a half times higher than that of the bare PBI membranes at each temperature. Besides, the H_2/CO_2 selectivity also shows an increase at 35 and 180 ^{0}C for the membranes containing ZIF-8, with a maximum value of 14.5. However, the selectivity value slightly decreases at 250 ^{0}C. This may be due to defects present in the membrane related to the integration of ZIF-8 that determine the flow at a higher temperature. The apparent activation energy was calculated for H_2, the fastest permeating compound in the binary mixture, resulting in values of 22.3 kJ/mol for the pure polymer and 19.5 kJ/mol for the MMMs (see Fig. S6). The apparent activation energy was also calculated for CO_2. This value slightly increased from 15.6 kJ/mol (bare polymer) to 16.3 kJ/mol when ZIF-8 was embedded in PBI. Both results are consistent with the increase in the H_2/CO_2 selectivity observed for most membranes at high temperature.

3.4 Influence of feed pressure on the gas separation performance

As previously mentioned, the increase in the feed pressure led to an enhancement of the gas separation performance. For example, the supported PBI membranes healed with PDMS showed the best results at 250 ^{0}C and 6 bar, with a H_2 permeation of 20.3 GPU and an H_2/CO_2 selectivity of 35.6 (see Fig. 4b). This means an increase of 29 % in the H_2 permeation while the H_2/CO_2 selectivity almost triples in comparison with the results of the same membrane at 3 bar. In the case of the ZIF-8 MMM, the H_2/CO_2 selectivity rises from 12.9 to 22.3 and the highest H_2 permeance of 22.4 GPU is reached. Defects produced by the integration of ZIF-8 into the PBI may be behind this behavior. In any event, the H_2/CO_2 selectivity almost doubles while the H_2 permeance rises by 18 %.

For a better understanding of the influence of the feed pressure on the gas separation performance of the different membranes tested, the permeation flows (m^3(STP)·m^2 (membrane)·s^{-1}) of H_2 and CO_2 measured in the permeate were represented as a function of the feed pressure. As shown in Fig. 5, the feed pressure has a clear influence on the gas separation performance depending on the nature of the PBI membranes. Regarding the PBI dense membranes, both H_2 and CO_2 flows increased almost equally with the increase in pressure resulting in a constant H_2/CO_2 separation factor. In the case of PBI uncoated asymmetric membranes, the H_2 flow increased more than that of CO_2, leading to a higher separation factor.

Finally, for PBI membranes healed with PDMS the flow of CO_2 remained constant as a function of the pressure while the H_2 flow increased. The small thickness of their skin layer caused the membranes to reach CO_2 saturation (Langmuir regime versus that of Henry in the two previous situations), significantly increasing the separation factor. Moreover, the PDMS coating healed the membrane defects avoiding possible viscous flow. CO_2 adsorption experiments in Figure S7 proved that the adsorption capacity of the asymmetric PBI membrane, with a more porous structure (as the SEM observation revealed), is tenfold higher than that of the dense membrane, making the former more suitable for CO_2 saturation at higher pressures. This result is in agreement with the dual-sorption model, which asserts that Henry sorption is the main mechanism of sorption into the matrix component, while Langmuir sorption governs the sorption into the microvoid region [51].

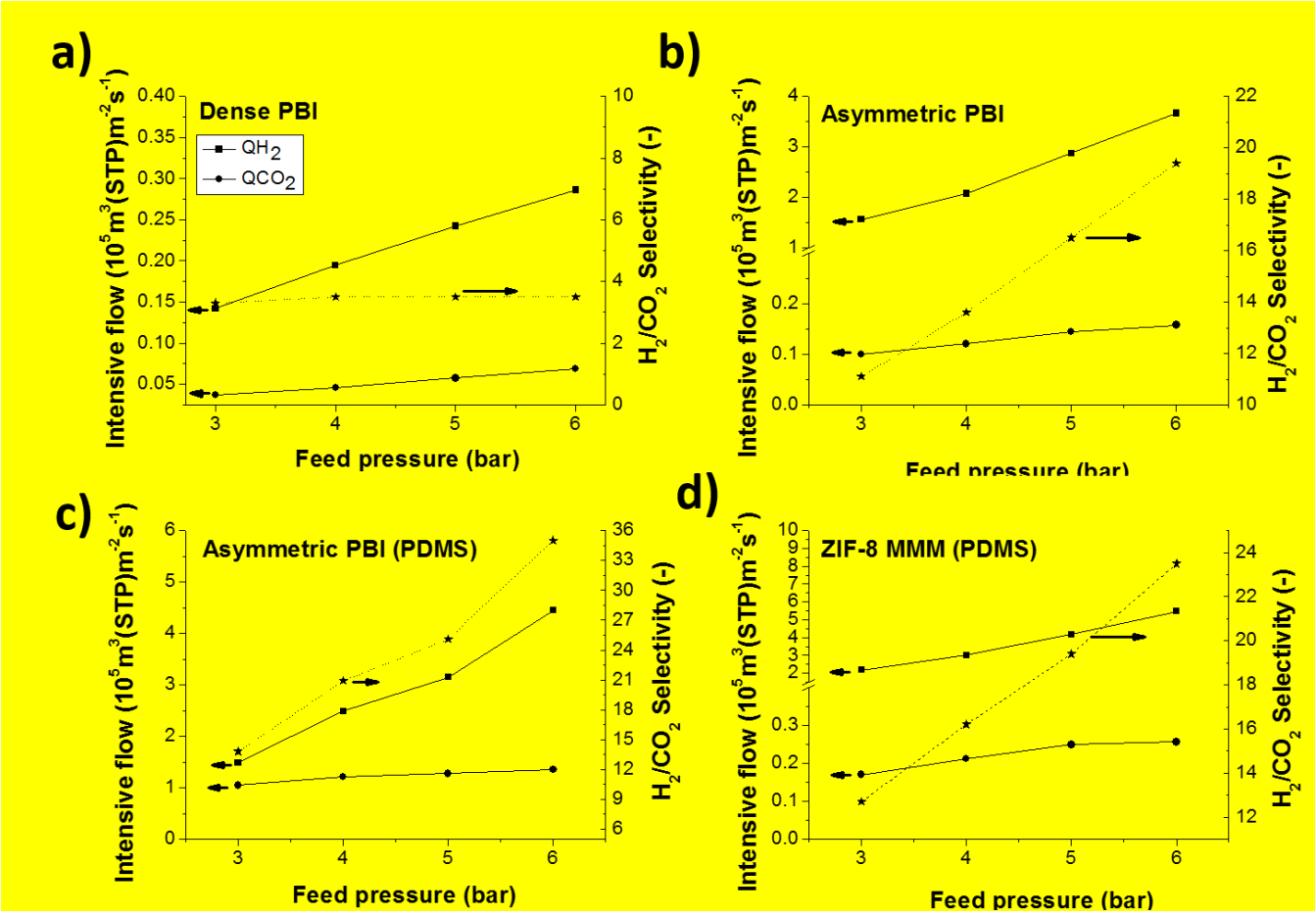

Figure 5. Gas separation performance for the separation of H_2/CO_2 binary mixtures of flat PBI membranes, dense (a) and asymmetric before (b) and after coating with PDMS(c) and asymmetric ZIF-8 MMM healed with PDMS (d) at different operating pressures. Intensive flows H_2 and CO_2 in $m^3(STP)\cdot m^2$ (membrane)$\cdot s^{-1}$ are given. (a) was tested at 150 °C while (b), (c) and (d) at 250 °C.

A similar tendency can be seen for ZIF-8 MMMs in dense and asymmetric configurations (Fig. S8 and 5d, respectively). The dense MMMs show a constant selectivity due to a parallel increase in both H_2 and CO_2 gas flows. In contrast, the asymmetric MMMs show an improvement in the selectivity with increasing feed pressure. Compared to neat asymmetric PBI membranes, the CO_2 flow is higher, making the H_2/CO_2 selectivity values decrease. This may be related to the relatively poor adsorption capacity of ZIF-8 (ca. 1.2 mmol/g at 100 kPa and 273 K) together with the shape of its adsorption isotherm (see Fig.

S7). The lack of a flattened portion in the curve, contrary to the tendency of the asymmetric PBI isotherm, means that ZIF-8 is far from saturation.

3.5 Membrane calculations

Pesek and Koros [52] considered that if the selectivity of an asymmetric membrane was higher than 80% of the intrinsic selectivity of the dense film, the gas transport was mostly controlled by the solution/diffusion mechanism. The skin layer thickness can be estimated from the ratio of gas permeability measured from the flat membrane and the hollow fiber permeance under the same testing conditions. The thickness of the asymmetric PBI membranes of this work was calculated from the gas permeation data at 180 ^{0}C and a feed pressure of 3 bar (Fig. 4a) using Eq 1:

$$l\ (\mu m) = \frac{H_2\ Permeability\ (Barrer)}{H_2\ Permeance\ (GPU)} \qquad \text{(Eq. 1)}$$

where the permeability represents the intrinsic permeation property of the polymeric material obtained from experiments with PBI dense membranes of known thickness. The calculated skin layer thickness for the self-supported and supported membranes were 15.2 and 2.1 μm, respectively. These values are in agreement with the SEM images in Fig. 1.

Fig. 4a shows how PBI supported asymmetric membranes coated with PDMS have higher selectivity values than self-supported membranes. Thus, the substructure of the former may contribute to their overall selectivity. The contribution of the substructure to the overall resistance (reciprocal to the permeance) can be estimated using a resistance model, considering that the skin layer, substructure and PDMS coating are connected in series (Eq 2) [53]:

$$\alpha_{H_2/CO_2} = \frac{(\alpha_1)_{H_2/CO_2} + (\alpha_2)_{H_2/CO_2}\left[\frac{(R_2)_{H_2}}{(R_1)_{H_2}}\right] + (\alpha_3)_{H_2/CO_2}\left[\frac{(R_3)_{H_2}}{(R_1)_{H_2}}\right]}{1 + \left[\frac{(R_2)_{H_2}}{(R_1)_{H_2}} + \frac{(R_3)_{H_2}}{(R_1)_{H_2}}\right]} \quad \text{(Eq. 2)}$$

where *1*, *2* and *3* refer to the resistance/selectivity of the skin layer, the substructure and PDMS coating, respectively. The known values in this equation, obtained from Fig. 4a, are: (*i*) those of the skin layer, considered the same as for self-supported asymmetric PBI ($(\alpha_1)_{H_2/CO_2} = 9.5$ and $R_1 = 1/2.1\ GPU^{-1}$); (*ii*) the overall selectivity of the supported PBI asymmetric membrane ($\alpha_{H_2/CO_2} = 12.6$); and (*iii*) the values for PDMS ($R_3 = 1/1500\ GPU^{-1}$ and $(\alpha_3)_{H_2/CO_2} = 0.8$), obtained from the literature [54]. Considering Kundsen selectivity as the substructure selectivity ($(\alpha_2)_{H_2/CO_2} = 4.7$), the calculated substructure layer resistance is 0.24 GPU^{-1}, meaning 33 % of the total resistance of the membrane.

The contribution of the substructure to the overall resistance in the MMMs at 180 °C can also be estimated using Eq 2. In this case the known values, different from the previous calculation, are: (*i*) those of the skin layer, obtained from the literature [14] ($(\alpha_1)_{H_2/CO_2} = 18$ and $R_1 = 1/3.0\ GPU^{-1}$) and (*ii*) the overall selectivity obtained from Fig. 4 ($\alpha_{H_2/CO_2} = 14.5$). The estimated substructure layer resistance was 0.12 GPU^{-1}, thus, 26 % of the total resistance of the membrane. The reduction in this resistance value compared to that of bare PBI membranes (33 %) may suggest that the filler is also somehow dispersed in the PBI substructure and not only located in the skin layer. The additional porosity of the ZIF-8/PBI composite, caused by the incorporation of the filler nanoparticles, enhances the diffusion of gases in the PBI layer, decreasing the flow resistance. Besides, the decrease in both the substructure resistance and the activation energy of H_2 may explain how the filler can be useful for the flow increase but not for an increase in the H_2/CO_2 selectivity (as seen in Fig. 4 and 5).

4. Conclusions

Asymmetric PBI flat membranes have been studied in this work. Neat polymeric membranes and ZIF-8 MMMs were prepared with this configuration. The concentration of the polymer dope strongly influenced the skin layer thickness and the mechanical resistance of the membrane. Dopes at 26 wt% led to self-supported and defect-free membranes, while 20 wt% dopes resulted in PBI membranes that needed a P84® support and PDMS healing. Characterization by SEM and Raman revealed that the latter membranes were constituted by a thin skin layer of around 1 μm on a finger-like macroporous structure. ZIF-8 was also successfully embedded in the polymer phase creating asymmetric PBI MMMs, with the nanoparticles clearly visible in the membrane cross-section. The necessary amount of ZIF was 2.5 fold smaller in comparison with equally loaded dense membranes. The membranes were tested for H_2/CO_2 pre-combustion mixed-gas separation up to 250 °C and 6 bar of feed pressure. The asymmetric PBI showed a better gas separation performance than PBI dense membranes, thanks to the different polymeric structure of the skin layer with this new membrane configuration. Embedding ZIF-8 into the PBI helped to enhance the gas separation performance of the membranes. Increasing the feed pressure had a positive effect on the performance of membranes with a thin skin layer. While the H_2 flow increased constantly with pressure, high pressures had a saturating effect on the CO_2 adsorption. This led to a change from the Henry to Langmuir regime that allowed a huge H_2/CO_2 selectivity increase. The substructure layer resistance in neat polymeric membranes was 33 % of the total resistance of the membrane. For the MMMs this value was slightly smaller (26 %). The same occurred with the calculated activation energy of the membranes, which decreased for H_2 when ZIF-8 was incorporated. Both facts indicate that the filler may only be useful in MMMs to increase the permeation flow.

Acknowledgments

The research leading to these results has received funding from the European Union Seventh Framework Programme (FP7/2007-2013) under grant agreement n° 608490, project M4CO2. In addition, financial support from the Spanish MINECO and FEDER (MAT2016-77290-R), the Aragón Government (T05) and the ESF is gratefully acknowledged. J. S-L. thanks the Spanish Education Ministry Program FPU2014 for his PhD grant. All the microscopy work was done in the Laboratorio de Microscopías Avanzadas at the Instituto de Nanociencia de Aragón (LMA-INA). Finally, the authors would like to acknowledge the use of the Servicio General de Apoyo a la Investigación-SAI, Universidad de Zaragoza.

References

[1] Z. Dai, L. Ansaloni, and L. Deng. Precombustion CO_2 Capture in Polymeric Hollow Fiber Membrane Contactors Using Ionic Liquids: Porous Membrane versus Nonporous Composite Membrane. Ind. Eng. Chem. Res, 55 (2016) 5983.

[2] S. Lee, J. Kang, K.T. Leung, W. Lee, D. Kim, S. Han, et al. Unique multi-phase Co/Fe/$CoFe_2O_4$ by water–gas shift reaction, CO oxidation and enhanced supercapacitor performances. J. Ind. Eng. Chem., 43 (2016) 69.

[3] J. Franz, P. Maas, and V. Scherer. Economic evaluation of pre-combustion CO_2-capture in IGCC power plants by porous ceramic membranes. Appl. Energy, 130 (2014) 532.

[4] Z. Ali, F. Pacheco, E. Litwiller, Y. Wang, Y. Han, and I. Pinnau. Ultra-selective defect-free interfacially polymerized molecular sieve thin-film composite membranes for H_2 purification. J. Mater. Chem. A, (2018) 30.

[5] M. Sadeghi, M.A. Semsarzadeh, and H. Moadel. Enhancement of the gas separation properties of polybenzimidazole (PBI) membrane by incorporation of silica nano particles. J. Membr. Sci., 331 (2009) 21.

[6] S. Kumbharkar, M.N. Islam, R. Potrekar, and U. Kharul. Variation in acid moiety of polybenzimidazoles: investigation of physico-chemical properties towards their applicability as proton exchange and gas separation membrane materials. Polymer, 50 (2009) 1403.

[7] T. Chung. A critical review of polybenzimidazoles: historical development and future R&D. J. Macromol. Sci., Part C: Polymer Rev., 37 (1997) 277.

[8] R.W. Baker. Overview of membrane science and technology. Membr. Technol. Appl., Second Edition, (2004) 1.

[9] S. Loeb, S. Sourirajan. Saline Water Conversion-II. Adv. Chem. Ser. , 38 (1963) 117.

[10] V. Giel, Z. Morávková, J. Peter, and M. Trchová. Thermally treated polyaniline/polybenzimidazole blend membranes: Structural changes and gas transport properties. J. Membr. Sci., 537 (2017) 315.

[11] V. Giel, M. Perchacz, J. Kredatusová, and Z. Pientka. Gas Transport Properties of Polybenzimidazole and Poly (Phenylene Oxide) Mixed Matrix Membranes Incorporated with PDA-Functionalised Titanate Nanotubes. Nanoscale Res. Let. , 12 (2017) 3.

[12] H.S.M. Suhaimi, C.P. Leo, and A.L. Ahmad. Hydrogen Purification Using Polybenzimidazole Mixed-Matrix Membranes with Stabilized Palladium Nanoparticles. Chem. Eng. Technol., 40 (2017) 631.

[13] J.R. Klaehn, C.J. Orme, and E.S. Peterson. Blended polybenzimidazole and melamine-co-formaldehyde thermosets. J. Membr. Sci., 515 (2016) 1.

[14] X. Li, R.P. Singh, K.W. Dudeck, K.A. Berchtold, and B.C. Benicewicz. Influence of polybenzimidazole main chain structure on H_2/CO_2 separation at elevated temperatures. J. Membr. Sci., 461 (2014) 59.

[15] T. Yang, T. Chung. High performance ZIF-8/PBI nano-composite membranes for high temperature hydrogen separation consisting of carbon monoxide and water vapor. Int. J. Hydrogen Energy, 38 (2013) 229.

[16] T. Yang, Y. Xiao, and T. Chung. Poly-/metal-benzimidazole nano-composite membranes for hydrogen purification. Energy Environ. Sci. , 4 (2011) 4171.

[17] S.C. Kumbharkar, P.B. Karadkar, and U.K. Kharul. Enhancement of gas permeation properties of polybenzimidazoles by systematic structure architecture. J. Membr. Sci., 286 (2006) 161.

[18] D.R. Pesiri, B. Jorgensen, and R.C. Dye. Thermal optimization of polybenzimidazole meniscus membranes for the separation of hydrogen, methane, and carbon dioxide. J. Membr. Sci., 218 (2003) 11.

[19] J. Sánchez-Laínez, B. Zornoza, S. Friebe, J. Caro, S. Cao, A. Sabetghadam, et al. Influence of ZIF-8 particle size in the performance of polybenzimidazole mixed matrix membranes for pre-combustion CO_2 capture and its validation through interlaboratory test. J. Membr. Sci., 515 (2016) 45.

[20] J. Sánchez-Laínez, B. Zornoza, C. Téllez, and J. Coronas. On the chemical filler–polymer interaction of nano-and micro-sized ZIF-11 in PBI mixed matrix membranes and their application for H_2/CO_2 separation. J. Mater. Chem. A, 4 (2016) 14334.

[21] R.P. Singh, G.J. Dahe, K.W. Dudeck, C.F. Welch, and K.A. Berchtold. High temperature polybenzimidazole hollow fiber membranes for hydrogen separation and carbon dioxide capture from synthesis gas. Energy Proc., 63 (2014) 153.

[22] K.A. Berchtold, R.P. Singh, J.S. Young, and K.W. Dudeck. Polybenzimidazole composite membranes for high temperature synthesis gas separations. J. Membr. Sci., 415 (2012) 265.

[23] S. Kumbharkar, K. Li. Structurally modified polybenzimidazole hollow fibre membranes with enhanced gas permeation properties. J. Membr. Sci., 415 (2012) 793.

[24] S. Kumbharkar, Y. Liu, and K. Li. High performance polybenzimidazole based asymmetric hollow fibre membranes for H_2/CO_2 separation. J. Membr. Sci., 375 (2011) 231.

[25] S.S. Hosseini, N. Peng, and T.S. Chung. Gas separation membranes developed through integration of polymer blending and dual-layer hollow fiber spinning process for hydrogen and natural gas enrichments. J. Membr. Sci., 349 (2010) 156.

[26] M.F. Flanagan, I.C. Escobar. Novel charged and hydrophilized polybenzimidazole (PBI) membranes for forward osmosis. J. Membr. Sci., 434 (2013) 85.

[27] R. Hausman, B. Digman, I.C. Escobar, M. Coleman, and T. Chung. Functionalization of polybenzimidizole membranes to impart negative charge and hydrophilicity. J. Membr. Sci., 363 (2010) 195.

[28] K.Y. Wang, Y. Xiao, and T. Chung. Chemically modified polybenzimidazole nanofiltration membrane for the separation of electrolytes and cephalexin. Chem. Eng. Sci., 61 (2006) 5807.

[29] S. Basu, A. Cano-Odena, and I.F. Vankelecom. Asymmetric Matrimid®/$[Cu_3\ (BTC)_2]$ mixed-matrix membranes for gas separations. J. Membr. Sci., 362 (2010) 478.

[30] H. Ren, J. Jin, J. Hu, and H. Liu. Affinity between metal–organic frameworks and polyimides in asymmetric mixed matrix membranes for gas separations. Ind. Eng. Chem. Res., 51 (2012) 10156.

[31] J. Van't Hof, A. Reuvers, R. Boom, H. Rolevink, and C. Smolders. Preparation of asymmetric gas separation membranes with high selectivity by a dual-bath coagulation method. J. Membr. Sci., 70 (1992) 17.

[32] S. Basu, A. Cano-Odena, and I.F. Vankelecom. MOF-containing mixed-matrix membranes for CO_2/CH_4 and CO_2/N_2 binary gas mixture separations. Sep. Purif. Technol., 81 (2011) 31.

[33] T. Chung, L.Y. Jiang, Y. Li, and S. Kulprathipanja. Mixed matrix membranes (MMMs) comprising organic polymers with dispersed inorganic fillers for gas separation. Prog. Polymer Sci., 32 (2007) 483.

[34] N. Nordin, A.F. Ismail, and A. Mustafa. Synthesis and preparation of asymmetric PSf/ZIF-8 mixed matrix membrane for CO_2/CH_4 separation. J. Teknol., 69 (2014) 73.

[35] T. Yang, G.M. Shi, and T. Chung. Symmetric and asymmetric zeolitic imidazolate frameworks (ZIFs)/polybenzimidazole (PBI) nanocomposite membranes for hydrogen purification at high temperatures. Adv. Energy Mater., 2 (2012) 1358.

[36] A. Bhaskar, R. Banerjee, and U. Kharul. ZIF-8@ PBI-BuI composite membranes: elegant effects of PBI structural variations on gas permeation performance. J. Mater. Chem. A, 2 (2014) 12962.

[37] N. Liédana, A. Galve, C. Rubio, C. Téllez, and J. Coronas. CAF@ ZIF-8: one-step encapsulation of caffeine in MOF. ACS Appl. Mater. Interfaces, 4 (2012) 5016.

[38] B.W. Rowe, L.M. Robeson, B.D. Freeman, and D.R. Paul. Influence of temperature on the upper bound: Theoretical considerations and comparison with experimental results. J. Membr. Sci., 360 (2010) 58.

[39] T. Chung, W.F. Guo, and Y. Liu. Enhanced Matrimid membranes for pervaporation by homogenous blends with polybenzimidazole (PBI). J. Membr. Sci., 271 (2006) 221.

[40] PBI Performance Products, Inc., Solutions brochure of "polybenzimidazole (PBI) S26 solution. https://pbipolymer.com/wp-content/uploads/2016/05/Celazole-PBI-S26-Typical-Properties.pdf

[41] T.S. Chung, S.K. Teoh, and X. Hu. Formation of ultrathin high-performance polyethersulfone hollow-fiber membranes. J. Membr. Sci., 133 (1997) 161.

[42] K.Y. Wang, T. Chung, and R. Rajagopalan. Dehydration of tetrafluoropropanol (TFP) by pervaporation via novel PBI/BTDA-TDI/MDI co-polyimide (P84) dual-layer hollow fiber membranes. J. Membr. Sci., 287 (2007) 60.

[43] C. Echaide-Górriz, S. Sorribas, C. Téllez, and J. Coronas. MOF nanoparticles of MIL-68 (Al), MIL-101 (Cr) and ZIF-11 for thin film nanocomposite organic solvent nanofiltration membranes. RSC Adv., 6 (2016) 90417.

[44] C. Echaide-Górriz, M. Navarro, C. Téllez, and J. Coronas. Simultaneous use of MOFs MIL-101 (Cr) and ZIF-11 in thin film nanocomposite membranes for organic solvent nanofiltration. Dalton Trans., 46 (2017) 6244.

[45] F. Conti, A. Majerus, V. Di Noto, C. Korte, W. Lehnert, and D. Stolten. Raman study of the polybenzimidazole–phosphoric acid interactions in membranes for fuel cells. Phys. Chem. Chem. Phys., 14 (2012) 10022.

[46] J. Young, W. Tsai, and F. Boerio. Characterization of the interface between pyromellitic dianhydride/oxydianiline polyimide and silver using surface-enhanced Raman scattering. Macromolecules, 25 (1992) 887.

[47] S.S. Hosseini, T.S. Chung. Carbon membranes from blends of PBI and polyimides for N_2/CH_4 and CO_2/CH_4 separation and hydrogen purification. J. Membr. Sci., 328 (2009) 174.

[48] X.Y. Chen, S. Kaliaguine, and D. Rodrigue. Correlation between performances of hollow fibers and flat membranes for gas separation. Sep. Purif. Rev., (2017).

[49] D.F. Sanders, Z.P. Smith, R. Guo, L.M. Robeson, J.E. McGrath, D.R. Paul, et al, Energy-efficient polymeric gas separation membranes for a sustainable future: A review, Polymer, 54 (2013) 4729.

[50] L.M. Robeson. The upper bound revisited. J. Membr. Sci., 320 (2008) 390.

[51] M. Askari, M.L. Chua, and T. Chung. Permeability, solubility, diffusivity, and PALS data of cross-linkable 6FDA-based copolyimides. Ind. Eng. Chem. Res., 53 (2014) 2449.

[52] S. Pesek, W. Koros. Aqueous quenched asymmetric polysulfone hollow fibers prepared by dry/wet phase separation. J. Membr. Sci., 88 (1994) 1.

[53] I. Pinnau, W.J. Koros. Relationship between substructure resistance and gas separation properties of defect-free integrally skinned asymmetric membranes. Ind. Eng. Chem. Res., 30 (1991) 1837.

[54] T. Merkel, R. Gupta, B. Turk, and B. Freeman. Mixed-gas permeation of syngas components in poly (dimethylsiloxane) and poly (1-trimethylsilyl-1-propyne) at elevated temperatures. J. Membr. Sci., 191 (2001) 85.

Figure captions

Figure. 4. SEM images of the cross-section of PBI self-supported asymmetric membranes fabricated from PBI dopes at 15 wt% (a), 20 wt% (b) and 26 wt% (c). PBI membrane skin layer thickness and PBI solution viscosity at 25 °C as function of PBI concentration in DMAc (d).

Figure 5. Raman spectra on different zones of the cross-section of a PBI supported membrane (left) together with its SEM image (right) with a zoom into the PBI skin layer (inset). The membrane was prepared from a 20 wt% PBI dope.

Figure 6. SEM image of the cross-section of a supported PBI asymmetric MMM with 10 wt% loading of ZIF-8 including EDX analysis (inset).

Figure. 4. Gas separation performance of dense PBI, self-supported asymmetric PBI, supported asymmetric PBI and asymmetric ZIF-8 10 wt% MMM. Histogram at 180 ^{0}C with feed and permeate pressures of 3 and 1 bar, respectively (a), and upper-bound plot (from 35 to 250 ^{0}C and pressure from 3 to 6 bar) with a comparison with hollow fiber literature values (in grey)[24-26] (b).

Figure 5. Gas separation performance for the separation of H_2/CO_2 binary mixtures of flat PBI membranes, dense (a) and asymmetric before (b) and after coating with PDMS(c) and asymmetric ZIF-8 MMM healed with PDMS (d) at different operating pressures. Intensive flows H_2 and CO_2 in $m^3(STP)\cdot m^2$ (membrane)$\cdot s^{-1}$ are given. (a) was tested at 150 °C while (b), (c) and (d) at 250 °C.